Journal of Applied Polymer Science

# Microstructure and Properties of Novel Fluorescent Pyrene Functionalized PANI/P(VDF-HFP) Blend

**Veer Pal Singh,[1] Ramasubbu Ramani,[1] Vijay Pal,[1] Asit Prakash,[2] Sarfaraz Alam[1]**

[1]Polymer Science Division, D.M.S.R.D.E., G.T. Road, Kanpur 208 013, India

[2]Department of Materials Science and Engineering, Indian Institute of Technology, Kanpur 208 016, India

Correspondence to: S. Alam (E-mail: sarfarazkazmi@yahoo.com)

**ABSTRACT:** We herein report the preparation and properties of the first polymer blend using pyrene functionalized polyaniline (pf-PANI). The pf-PANI has been synthesized and its blend has been prepared with the copolymer of vinylidene fluoride and hexafluoropropylene P(VDF-HFP). The FTIR results reveal intermolecular interaction between the polar amide group of pf-PANI and the polarized $CH_2$ group of P(VDF-HFP). The crystalline phase of PVDF of the copolymer revealed a transformation from $\alpha$ to $\beta$ crystalline form after blending with pf-PANI, as found from FTIR and XRD measurements. The calorimetric measurements together with DMA results revealed the blend is partially miscible. The SEM measurements showed that the pf-PANI has been dispersed uniformly in the P(VDF-HFP) matrix. The solution photoluminescence spectrum of the pf-PANI exhibited emission in the purple–blue region and is slightly red shifted for the blend. The possible applications of this flexible fluorescent pf-PANI/P(VDF-HFP) has been suggested.
 J. Appl. Polym. Sci. **2014**, *131*, 40163.

**KEYWORDS:** pyrene functionalization; polyaniline; poly(vinylidene fluoride-co-hexafluoro propylene); polymer blend; X-ray diffraction

Received 7 July 2013; accepted 1 November 2013

**DOI: 10.1002/app.40163**

## INTRODUCTION

Fluoropolymers such as poly(vinylidene fluoride) (PVDF) and its copolymers are technologically important thermoplastics because of their availability in different crystalline forms.[1] The incorporation of amorphous phase of hexafluoropropylene (HFP) into the main constituent vinylidene fluoride (VDF) blocks has been reported to modify some of the properties of the homopolymer. Particularly, the degree of crystallinity of P(VDF-HFP) is significantly reduced in comparison with PVDF, while the flexibility and solubility for organic solvents are enormously increased.[1,2] The amorphous HFP domains can trap more liquid electrolytes and the crystalline regions (of VDF) can help to maintain mechanical integrity of the film. On account of this merit, P(VDF-HFP) has received special attention as one of the promising host polymers for polymer electrolytes.[2–4] In addition, the dielectric permittivity of P(VDF-HFP) is also high as compared with other conventional polymers.[4]

Amongst conductive polymers, polyaniline (PANI) has received special attention since it possess excellent conductivity.[5] However, the processibility of PANI has been a crucial factor in making use of its interesting electrical and electrochemical properties in real applications since it is insoluble in common organic solvents and is unstable at melt processing temperatures.[6,7] In addition, the molecular weight of PANI is relatively poor in comparison with other conventional polymers.[6] Thus, blending PANI with other conventional polymers, could lead to blend with excellent mechanical properties and high processibility of the conventional polymers together with the electrical conductivity of PANI. This could increase the technological potential and the commercial viability of PANI.[8,9] Keeping this aspect in view, successful blends have been prepared in the past with conventional polymers like poly(vinyl acetate),[10] poly(-methyl methacrylate) (PMMA),[11] polystyrene,[12] polycarbonate,[13] poly(ethylene terephthalate)[14] as well as with copolymer poly(ethylene-*co*-vinyl acetate)[8] thus leading to materials of high mechanical strength and with good electrical conductivity.

But, previous attempts to prepare blends of PANI with PVDF by mixing them in common solvent turned out to be unsuccessful (as PANI precipitated forming a two-phase system).[6] The miscibility between PANI and PVDF has been suggested to improve by adding poly(vinyl chloride)[15] which however resulted to low mechanical strength and conductivity. But, the derivatives of PANI like poly(*o*-methoxyaniline) and poly(*o*-ethoxyaniline) and PVDF are reported to be miscible because of the presence of polar groups in these PANI derivatives.[6,16] An alternate method to obtain PANI/PVDF blends has been reported in which the oxidative polymerization of aniline is performed in solution of PVDF using P-toluene sulfonic acid (p-

TSA) as a dopant and the blend is reported to be homogeneous and good mechanical stability.[5] Successful works on the binary blend has motivated researchers to go for ternary blends composed of PVDF/PMMA/PANI using DBSA as a dopant.[9] In the recent past, researchers have succeeded in making PANI/PVDF blend without additives using combined grinding-cast procedure for dielectric capacitor applications.[17]

The PVDF is generally compatible with polymers having ⟩C═O groups in general and particularly with polymer having ⟩C═O groups in its side chain since the highly polarized $CH_2$ group of the VDF can form hydrogen bonds with the ⟩C═O groups.[18] Because of this ability of hydrogen bonding interaction, compatible blends of PVDF have been made in the past with PMMA and acrylic resins.[11,18] Recently, pyrene functionalized PANI has been reported that carries two ⟩C═O groups in its side chain[19] (see Scheme I). Also, pyrene functionalization to PANI backbone results to material with good light emitting property and better solubility in organic solvents as compared with PANI.[19] Thus, it is anticipated that even P(VDF-HFP) will be compatible with pf-PANI. Furthermore, there has been an increased interest in the use of pyrene for organic electronic applications owing to its interesting properties and more details on this subject can be obtained in the recent review.[20] In this work, the thermal, viscoelastic behavior, crystalline structure, morphology and optical properties of pf-PANI/P(VDF-HFP) are studied in comparison with its reference counterparts, raising the technological importance of this blend. To the best of our knowledge, this is the first report on polymer blend using pyrene functionalized polyaniline (pf-PANI).

## EXPERIMENTAL

### Sample Preparation

Pellets of copolymer of VDF and hexafluoropropylene P(VDF-HFP) having $M_w = 400{,}000$ g/mol and $M_n = 130{,}000$ g/mol used in this study, was obtained from Sigma-Aldrich. Henceforth, this copolymer will be termed as PVH. The PVH was dried in vacuum at 50°C for 24 h before use. All the chemicals used in this study were also obtained from Sigma-Aldrich. The chemicals such as ammonium persulphate, sodium hydroxide, and hydrochloric acid were used without further purification while aniline, *m*-cresol and N-methyl-2-pyrrolidinone (NMP) were double distilled before use.

The structure of PANI is popularly called as *para*-linked phenylene amine-imine. The PANI derives from the general formula $[(\text{—B—NH—B—NH—})_y\ (\text{—B—N═Q═N—})_{1-y}]_n$ in which B and Q denote benzene rings in the benzenoid and quinonoid forms, respectively. In case of PANI, the oxidation states can vary from that of the fully reduced state ($y = 1$) called leucoemeraldine (LM); 50% intrinsically oxidized state ($y = 0.5$) called emeraldine base (EB); to that of the fully oxidized ($y = 0$) called pernigraniline (PNA). The polymer can achieve its highly conductive state either through protonation of the imine nitrogens (═N—) in its EB state or through the oxidation of amine nitrogens (—NH—) in its LM state.[21]

The EB form of PANI (PANI-EB) was synthesized using a standard procedure[22] and is the starting material for pyrene functionalized PANI (pf-PANI) synthesis. The pf-PANI has been synthesized by following the method as reported.[19] In brevity, the synthesis was done by dissolving PANI base in *m*-cresol solvent and made to react with acid chloride of pyrene butyric acid at 120°C for 12 h to form pf-PANI. The HCl formed during pf-PANI synthesis acted as a dopant to the PANI chain and could not be removed even after prolonged washing process. This resulted to protonation of the imine part of PANI backbone. The formed pf-PANI was precipitated with methanol, dried for 48 h in air and then in vacuum for another 24 h before use in the preparation of blend. The pf-PANI/PVH blend was prepared by mixing pf-PANI and PVH in NMP solvent (1 wt % solution) so as to form blend with equal weight ratio. The mixing was continued for 24 h and the solvent was evaporated thoroughly in air for 48 h and then kept in vacuum for overnight. The chemical structure of the pf-PANI, PVH, and the possible interaction site between them in their blend is shown in Scheme I.

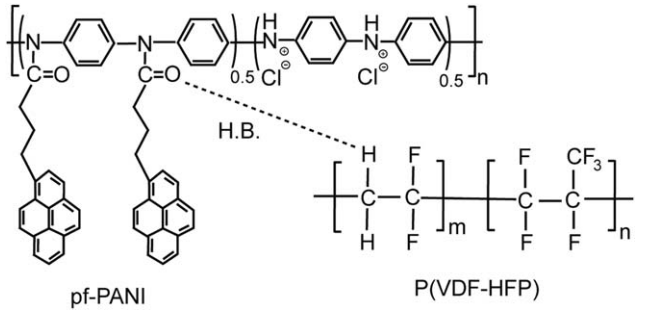


**Scheme I.** Chemical formulas of pf-PANI and P(VDF-HFP) as well as the possible interaction site between them has been schematically shown.

### Characterization

**Fourier Transform Infrared Spectroscopy.** An FTIR spectrophotometer of PerkinElmer (model Spectrum 100) was used to identify the chemical structure of the polymers and the blend. The samples were grinded with KBr powder using a pestle and mortar and pressed to pellets. The samples were then dried in the vacuum oven atleast for 12 h before the infrared spectra were recorded.

**Thermogravimetric Analysis.** Thermo gravimetric analysis was performed using a TGA instrument (Mettler–Toledo TGA/SDTA 851$^e$) in the temperature range 30–800°C. Thermal decomposition experiments were carried out in dynamic conditions using samples of ca. 5 mg and a heating rate of 20°C/min both in argon and dry air atmosphere (flow rate = 50 mL/min).

**Differential Scanning Calorimetry.** The glass transition temperature ($T_g$), melting temperature ($T_m$), crystallization temperature ($T_c$) and associated enthalpy changes were measured using a DSC equipment of TA instruments (Q 200 DSC) in nitrogen atmosphere (flow rate = 50 mL/min). The instrument is equipped with a refrigerated cooling system and has a temperature accuracy of ±0.1°C. Samples of ~5 mg were weighed and sealed in aluminum sample pans and were heated above their melting temperature for 5 min in a conventional manner to erase the thermal history. The samples were reheated from −90°C to 250°C @ 10°C/min and cooled. The data from the second heating and cooling traces are reported here.

**Modulated Differential Scanning Calorimetry.** To confirm the results of DSC measurements, separate MDSC measurements were also performed to elucidate the $T_g$ based on the change in reversible $C_p$ ($C_p^{rev}$) and its temperature derivative ($dC_p^{rev}/dT$) with temperature. The modulation temperature amplitude was kept small (0.32°C) relative to the underlying heating rate (2°C/min), so that no local cooling during the standard MDSC scan (heating-only) and the modulation period was kept as 60 sec. The peak temperature of $[dC_p^{rev}/dT]$ is equated to the middle of the step-change in $C_p^{rev}$ curve.

**Dynamic Mechanical Thermal Analysis (DMTA).** The viscoelastic behavior of the samples were studied in the film form in tension mode using a DMTA of GABO (EPLEXOR—150N). The dynamic responses were tested from −100°C to 120°C at a frequency of 10 Hz and with a heating rate of 2°C/min.

**Wide Angle X-ray Scattering (WAXS).** The WAXS patterns were collected with a X-ray Diffractometer of Rich Seifert & Co., Germany (model ISO-Debyeflex 2002) using Cu $K_\alpha$ radiation ($\lambda = 1.54$ Å). The samples were placed between the kapton foils and the scattering profiles were collected at diffraction angle $2\theta$ from 5° to 60° at a scanning rate of 1°/min to explore the crystalline structure of the virgin polymers and their blend.

**Scanning Electron Microscopy (SEM).** The surface morphology of the blends was examined using a Carl Zeiss EVO 50 Scanning Electron Microscope with 10 kV operating voltage. The samples were sputter coated with gold on the viewing surface to enhance its conductivity.

**UV–Visible Spectroscopy.** The optical absorption measurements of the samples were carried out using quartz cuvettes at room temperature in NMP solution (0.01 mg/mL) using a UV–Vis spectrophotometer of Thermoscientific (model GEESYS 10S).

**Photoluminescence Spectroscopy.** The photoluminescence (PL) experiments were also recorded in NMP solution (0.005 mg/mL) using a Horiba Jobin Yvon FluoroLog-3 Spectrofluorometer. The photoexcitation was done at the wavelength corresponding to maximum absorbance by the polymer. The emission was detected at right angles to the direction of excitation.

## RESULTS AND DISCUSSION

First, we report the confirmatory tests for the synthesized pf-PANI and compare the results with PANI-EB. The UV–Visible measurements for PANI-EB when collected in chloroform solvent (0.4 mg/mL), revealed strong absorption bands at ca. 270 nm, 386 nm, and 560 nm. The absorption at 560 nm is due to quinonoid form of benzene ring while the absorption at 386 nm is due to benzenoid form.[5,7,21] In case of pf-PANI in chloroform solvent (0.01 mg/mL), the absorption bands seen at ca. 246 nm, 280 nm and 348 nm are the characteristic absorptions of pyrene functionalized moieties [see Figure 1(A)].[23] Please note that PANI-EB is sparingly soluble in chloroform and its concentration needs to be relatively high as compared with pf-PANI to get an optimum UV–Vis spectrum. The PL measurements for pf-PANI upon excitation at 355 nm in m-cresol solution (0.005 mg/mL) reveal an excimer fluorescent intensity maximum at ca. 479 nm in close agreement with its reported value [see Figure 1(B)][19,23] while PANI-EB exhibits PL intensity maximum at ca. 398 nm.

The molecular structure of the pf-PANI is further confirmed by FTIR measurements. The FTIR spectrum of PANI-EB and pf-PANI are displayed in Figure 1(C). The ring stretching of the quinonoid and benzenoid form of benzene in PANI are clearly observed at 1581 and 1477 $cm^{-1}$, respectively.[24,25] The presence of almost equal intensities for 1477 $cm^{-1}$ and 1581 $cm^{-1}$ bands is consistent with the PANI structure in its EB state.[21] The C—N stretch of the aromatic amine appears at ca. 1295 $cm^{-1}$.[7,19] In addition, pf-PANI exhibits the aliphatic asymmetric and symmetric C—H stretch vibrations at 2952 and 2856 $cm^{-1}$, respectively indicating the existence of alkyl substituents in PANI chain.[7] The ⟩C═O stretch vibration in pf-PANI appears at ca. 1651 $cm^{-1}$, due to N-[4-(1′-pyreno butanoyl)] group attached to PANI (see Scheme I). The resulting structure leads to an amide group in pf-PANI. It is known in polymers and peptides that the ⟩C═O stretch of the amide (amide I band) occurs at ca. 1650 $cm^{-1}$.[26,27] It is good to note that this ⟩C═O stretch band is distinctly seen even though there is an overlapping quinonoid ring stretch band [Figure 1(C)]. Also, the 1156 $cm^{-1}$ band seen in pf-PANI is the characteristic of the doped (protonated) imine part of PANI,[21] which indicates that the [4-(1′-pyreno butanoyl)] group is attached to the amine part (see Scheme I).

### FTIR Results

The molecular interactions between pf-PANI and PVH have been analyzed using FTIR spectrum (Figure 2). Depending on the geometric chain configurations, the crystalline structure of PVDF can exist mainly as α and β forms.[1] The α-form has *trans* and *gauche* conformations arranged as TGTG' with the neighbouring dipole moments in opposite directions, and thus the unit cell has no net dipole. The β-form has all *trans* confirmations and more polar than α-form.[1,27] The features observed at 615 and 763 $cm^{-1}$ in virgin PVH are due to α crystalline phase of PVDF.[1,27] The spectral feature at 615 $cm^{-1}$ is attributed to a mixed mode of $CF_2$ bending and C—C—C skeletal vibration while the one at 763 $cm^{-1}$ is attributed to in-plane bending vibration.[1] These features are absent in the blend. Instead, strong peaks at 510, 840, and 879 $cm^{-1}$ are evident for the blend which is due to β crystalline phase of PVDF.[1,4,27] The 510 $cm^{-1}$ has been assigned to $CF_2$ bending mode, 840 $cm^{-1}$ peak has been assigned to a mixed mode of $CH_2$ rocking and $CF_2$ asymmetric stretching vibration and 879 $cm^{-1}$ is assigned to $CF_2$ stretch of PVDF-HFP.[1] Thus, the FTIR results indicate the possible transformation of PVDF (in PVH) from α-crystalline form to β-form upon blending it with pf-PANI. We confirm this transformation also from our XRD results, which will be discussed below.

The amide I band at 1600–1700 $cm^{-1}$ is the characteristic ⟩C═O stretch and infers whether the ⟩C═O group participates in the hydrogen bonding or not.[28] As pointed out earlier, the spectral feature seen at ca. 1651 $cm^{-1}$ in pf-PANI is the contribution from ⟩C═O stretch of the amide linkage. This band

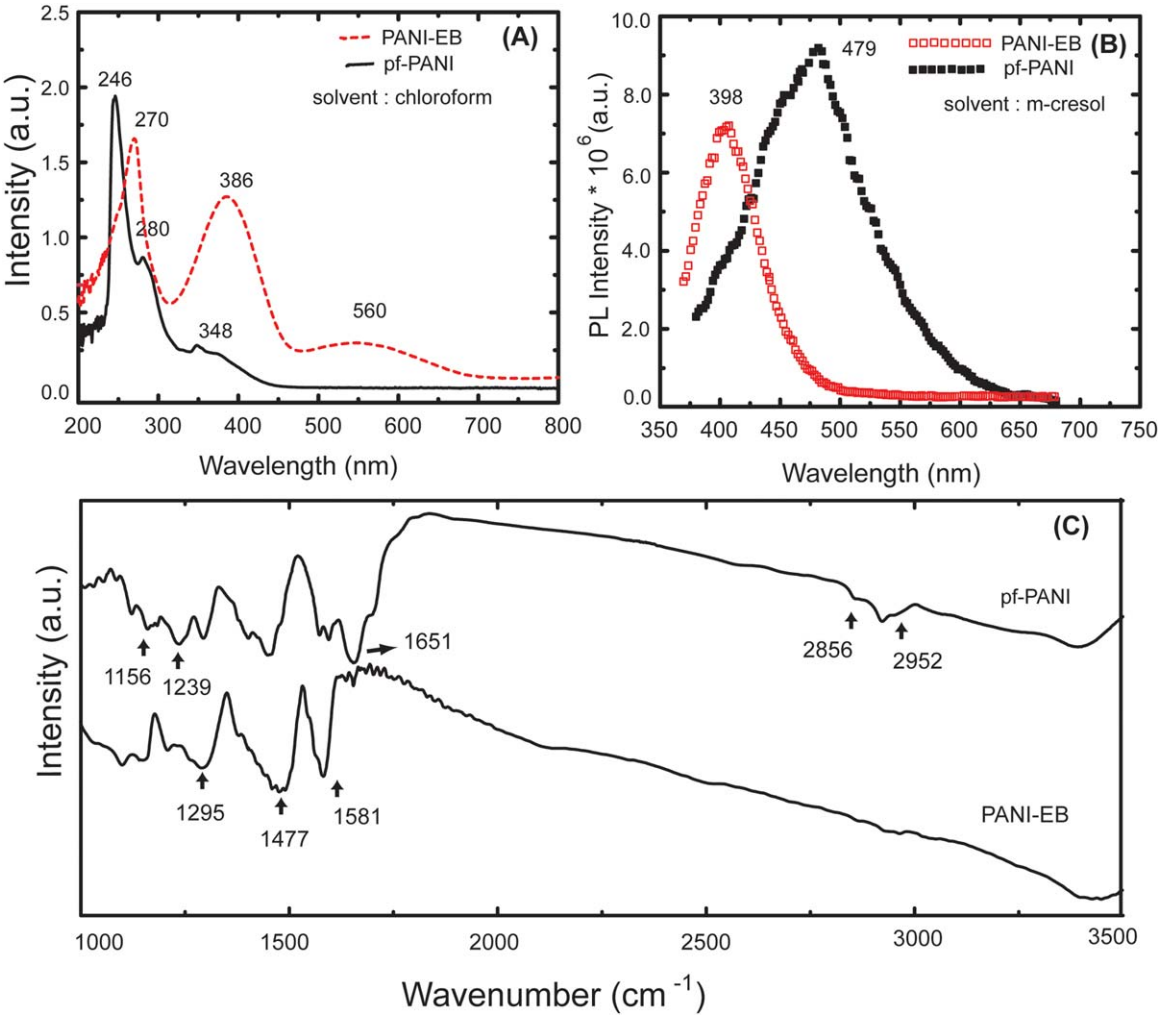


**Figure 1.** (A) UV–Vis spectrum of PANI-EB (0.4 mg/mL) and pf-PANI (0.01 mg/mL) collected in chloroform solution (B) PL spectrum of PANI-EB and pf-PANI in m-cresol solution (0.005 mg/mL) and (C) A comparative FTIR spectra of pf-PANI and PANI-EB in the region 1000–3500 $cm^{-1}$. The FTIR spectra have been displaced vertically for clarity. [Color figure can be viewed in the online issue, which is available at wileyonlinelibrary.com.]

downshifts to 1644 $cm^{-1}$ when blended with PVH. It is known in polymers and peptides that the amide I band downshifts in wave number upon hydrogen bonding, while the free carbonyl group appears at higher wavenumber.[26–28] This observation can be interpreted in terms of probable interaction between the hydrogen in the $CH_2$ group of PVH and the oxygen of the ⟩C═O group of pf-PANI (see Scheme I).

In addition to this, there are other spectral features which support the interaction of pf-PANI and PVH. The intense peak at 1452 $cm^{-1}$ of pf-PANI almost disappears and a new peak emerges at 1404 $cm^{-1}$. The two sharp peaks at 1239 and 1291 $cm^{-1}$ together with the spectral feature seen at ca. 1156 $cm^{-1}$ in pf-PANI appears to have been merged and results to a single broad peak in the blend. It is to be noted that virgin PVH do not exhibit any strong overlapping spectral features in this region. Also, the peak at 806 $cm^{-1}$ in pf-PANI almost vanishes in the blend. All these spectral changes also indicate the interaction between pf-PANI and PVH exists.

**TGA Results**

The effect of pf-PANI inclusion on the thermal properties of PVH has been studied by TGA, DSC, MDSC, and DMTA. The TGA results of the virgin polymers and their blend are carried out in argon [Figure 3(A)] and in dry air [Figure 3(B)], respectively, and their corresponding derivative curves are shown in Figure 3(C,D). In argon medium, the PVH chain decomposes by random chain-scission at a temperature of ca. 440°C. This decomposition temperature is in good agreement with its reported value of 420–470°C for this copolymer by other research groups.[29–31] The pf-PANI exhibits two steps of mass loss behavior. In the first step, a small fraction of mass loss (<2%) gets initiated at ca. 170°C, which is attributed to evolution of acid or could be due to loss of oligomers and unbounded dopant.[32] The second and main decomposition step unlike the first step could be clearly deciphered and begins at ca. 220°C with a decomposition maximum at ca. 313°C which is attributed to cleavage of the alkyl tails and the decomposition

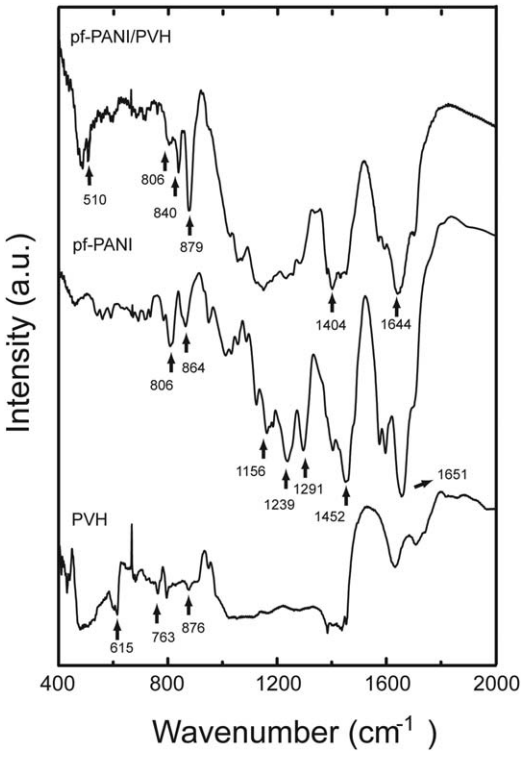


**Figure 2.** FTIR spectra of pf-PANI, PVH, and pf-PANI/PVH in the region 400–2000 $cm^{-1}$. For clarity, the spectra have been displaced vertically.

of the PANI main chain. Please note that the PANI-EB backbone degradation occurs at ca. 420°C and the doped PANI is less thermally stable than PANI-EB.[33] In the present case, the additional bulky side chains in pf-PANI have further reduced the thermal decomposition temperature to ca. 220°C. The char yield at 800°C is ca. 23% for the PVH while it is 38% for pf-PANI.

The TGA plot for the blend in the inert medium shows two-step decomposition and indicates the degradation features of both the partners with the decomposition maximum ($T_{max}$) at a slightly different temperature. This change in $T_{max}$ again supports the findings that the interaction between the two polymers exists. The first decomposition has a $T_{max}$ at ca. 320°C, which is slightly higher than the $T_{max}$ of the main decomposition of pf-PANI. The second decomposition has a $T_{max}$ at ca. 482°C which is slightly lower than the $T_{max}$ of PVH.

The decomposition of PVH in air medium is similar to that in argon medium atleast up to 440°C. The thermo-oxidation starts for PVH at ca. 440°C, which leads to almost negligible residue at 800°C. The pf-PANI shows three-step decomposition in air medium with the first two steps similar to the decomposition in inert medium while the third step is due to oxidation of the PANI backbone that gets initiated around 500°C with a decomposition maximum at ca. 572°C leaving almost no residue at 800°C. The blend exhibits the thermo-oxidation pattern similar to pf-PANI and PVH.

### DSC Results

The DSC plots of the samples during second heating and cooling are shown in Figure 4(A,B), respectively and the results are tabulated in Table I. The $T_g$ is one of the most important parameters of the amorphous phase that determines the flexibility of the material at room temperature. The reported $T_g$ value of pf-PANI is 210°C.[19] Infact, we observed a similar DSC curve as given in ref. 19 [data shown as an inset in Figure 4(A)]. But, upon second and third heatings, this transition does not exist but the step-change is observed at 87°C during these repeated heatings. Hence, we suggest that the transition seen during first heating could be associated with residual stress retained in the polymer during preparation conditions and the $T_g$ of pf-PANI is ca. 87°C. To confirm the $T_g$, we have also performed MDSC measurements and are discussed in the next section. It is interesting to note that pf-PANI exhibits no indication of melting or crystallization up to the decomposition temperature [220°C; see Figure 3(A)] and similar behavior has been observed in pyrene functionalized octavinylsilsequinone.[34]

The $T_g$ of virgin PVH is a weak transition occurs at ca. −32.6°C and the melting temperature ($T_m$) occurs at ca. 137°C which is close to that reported.[35,36] The blend showed no evidence of $T_g$ but the $T_m$ up shifts to ca. 143°C. The heat of fusion for pure PVH is 16.4 J/g while that for the blend it is 6.0 J/g (see Table I). The PVDF crystalline phase in $\beta$-form are characterized with higher $T_m$ as compared with $\alpha$–form.[1,37,38] Thus, the up shift in $T_m$ could be taken as the formation of strong $\beta$ crystalline structure, thus supporting the FTIR and WAXS results. Upon cooling, higher crystallization temperature is found for the blend (96°C) as compared with PVH (92°C), which suggests that the pf-PANI chains acts as a nucleating agent for PVH crystallization [Figure 4(B)]. This result is completely in contradiction to the results reported for PANI/PVDF blend, where the authors did not observe any change in $T_g$ and $T_m$ for the blend in comparison with their reference counterparts suggesting their incompatibility.[39]

Using the enthalpy value obtained for the melting of PVH, the relative crystallinity ($X_c$) of the blend is calculated as

$$X_c = \{\Delta H_m / \Delta H_m^{\circ}\} * 100\%,$$

where $\Delta H_m^{\circ}$ is the enthalpy change associated with the melting of 100% crystalline PVDF 105 J/g [40] and $\Delta H_m$ is the heat of fusion for the blend. Using this, the $X_c$ value for PVH is found to be 15.6% and it decreases to 5.7% for the blend. The decrease in $X_c$ is in agreement with the XRD results showing less crystalline peaks. This drop in crystallinity is ca. 64% to its original value which is higher than the composition of PVH in the blend (50%). This result also supports the fact that pf-PANI and PVH are compatible.

### MDSC Results

It is known that polymer blends that are judged miscible based on conventional DSC have shown two calorimetric $T_g$s based on heat capacity results obtained from MDSC[41,42] and thus the indication of a single $T_g$ in a blend using DSC is not the universal feature to judge the polymer miscibility.[41] To elucidate the presence of possible $T_g$s in these materials, $C_p^{rev}$ and its temperature derivative $[dC_p^{rev}/dT]$ are plotted against temperature [Figure 5(A,B)]. In the $[dC_p^{rev}/dT]$ versus temperature plot, only one peak is evident for pf-PANI (ca. 85°C) and PVH (ca. −30°C). However, the blend showed two peaks at ca. −20°C

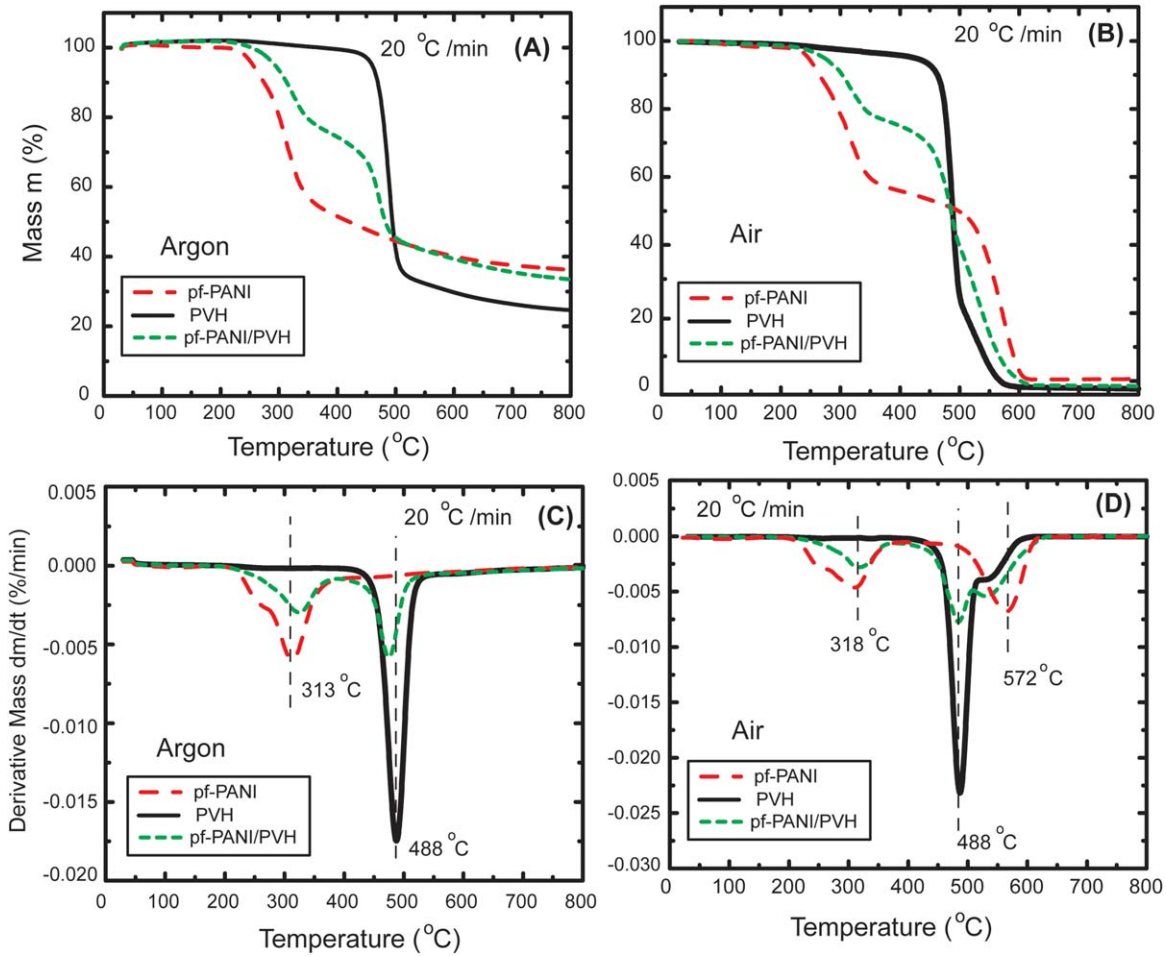


**Figure 3.** (A) Typical thermograms of pf-PANI, PVH and pf-PANI/PVH in the temperature range 30–800°C (A) in argon medium and (B) in air medium. Their respective derivative curves (C) in argon medium and (D) in air medium. [Color figure can be viewed in the online issue, which is available at wileyonlinelibrary.com.]

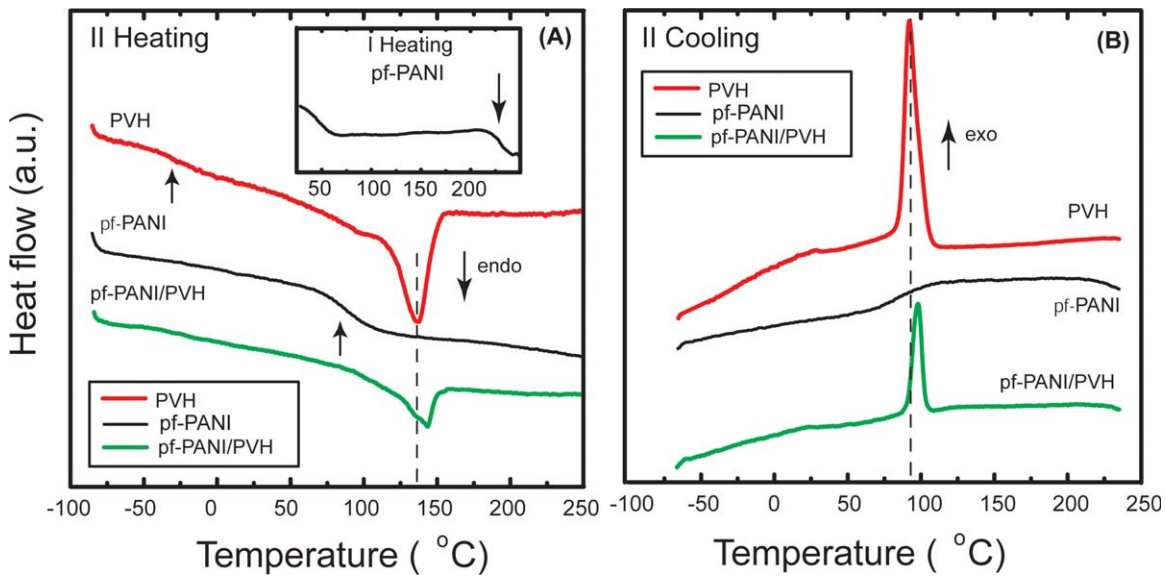


**Figure 4.** DSC thermograms of pf-PANI, PVH, and pf-PANI/PVH during (A) second heating and (B) second cooling. The thermograms are displaced vertically for clarity. The first heating curve for PANI-EB is shown in the inset of (A). [Color figure can be viewed in the online issue, which is available at wileyonlinelibrary.com.]

**Table I.** DSC and MDSC Results of pf-PANI, PVH, and pf-PANI/PVH Blend

| | DSC | | | | | MDSC |
|---|---|---|---|---|---|---|
| Sample | $T_g$ (°C) | $T_m$ (°C) | $\Delta H_m$ (J/g) | $T_c$ (°C) | $\Delta H_c$ (J/g) | $T_g$ (°C) |
| PVH | −32.6 | 137.7 | 16.4 | 92.1 | 23.9 | −30.2 |
| pf-PANI | +87.0 | - | - | - | - | +84.8 |
| pf-PANI/PVH | −22.0 | 143.2 | 6.0 | 96.2 | 9.9 | −20.2 and +49.8 |

and 50°C, thus revealing the presence of two $T_g$s (see Table I). The presence of two identifiable $T_g$s in the blend which are shifted towards each other from their original values infers that the blend is partially compatible.[43,44] Thus, the decrease in $T_g$ of pf-PANI and increase in the $T_g$ of PVH indicates some level of intermolecular interactions in the amorphous regions of the blend. It is to be noted that even the $T_g$ of PVH is not well resolved in DSC plot [Figure 4(A)], while it is distinctly evident in MDSC results [Figure 5(B)].

### DMTA Results

To further understand the glass transition process in these materials, their viscoelastic behavior was studied in the temperature region −100°C to 120°C using DMTA [see Figure 6(A,B)]. At low temperature region (−40°C to −100°C), the blend exhibits a storage modulus *E'* (7.6 GPa) almost comparable with the virgin PVH (8.8 Gpa). This *E'* value for PVH is in close agreement with the *E'* value of PVDF reported at −80°C.[39] Upon heating, the storage modulus for virgin PVH starts to decrease steadily at ca. −45°C while the blend retains its stiffness up to ca. −27°C but decreases steeply thereafter. Although the *E'* of both the PVH and the blend decreases in a different manner, their *E'* values reach to almost comparable state in the temperature region 20–40°C. In this temperature regime, *E'* for the blend shows a small plateau and start to decrease again beyond 40°C. In correlation with the results obtained from MDSC, this second decrease in *E'* could be attributed to the $T_g$ of the pf-PANI.

However, a film of pf-PANI alone could not be characterized with DMA owing to its brittle nature (see photographs of the representative films displayed as an inset in Figure 6(B). Please note that the brittle nature of pf-PANI has resulted to films of very small size and are arranged in a manner so as to appear similar to PVH and pf-PANI/PVH films). It is good to compare here an earlier DMA results on PANI/PVDF blend,[39] where the authors observed drop in *E'* value at −40°C for both virgin PVDF and its blend owing to their immiscibility.

The tan $\delta$ is widely being used to identify the $T_g$ of the polymers and their blends.[14] The pure PVH shows a single tan $\delta$ peak at ca. −3°C. Interestingly, the blend shows two peaks one at ca. 8°C and the other at ca. 90°C with a shoulder at the left part of the high temperature peak. Similar to *E'* variation with temperature indicating two $T_g$s for the blend, the low temperature peak is due to $T_g$ of PVH while the high temperature peak is related to $T_g$ of pf-PANI. The shoulder peak is suggested to represent the mixed amorphous phase of pf-PANI and PVH, thus revealing their partial compatibility as observed in other polymer blends.[45] It is interesting to note that even though the *E'* of both PVH and the blend almost decreases in a similar manner above 40°C, their tan $\delta$ shows a very different behavior. The tan $\delta$ peak height value for the blend reaches to almost thrice the value of PVH at this temperature. This suggests good ductile behavior of the blend as compared with pristine PVH. This result is interesting in comparison with an earlier work on blending PANI with PVDF that has resulted to blend with brittle nature.[21]

### WAXS Results

The XRD profiles of virgin PVH, pf-PANI and their blend are measured in the $2\theta$ range 5° to 60°. The data were smoothed

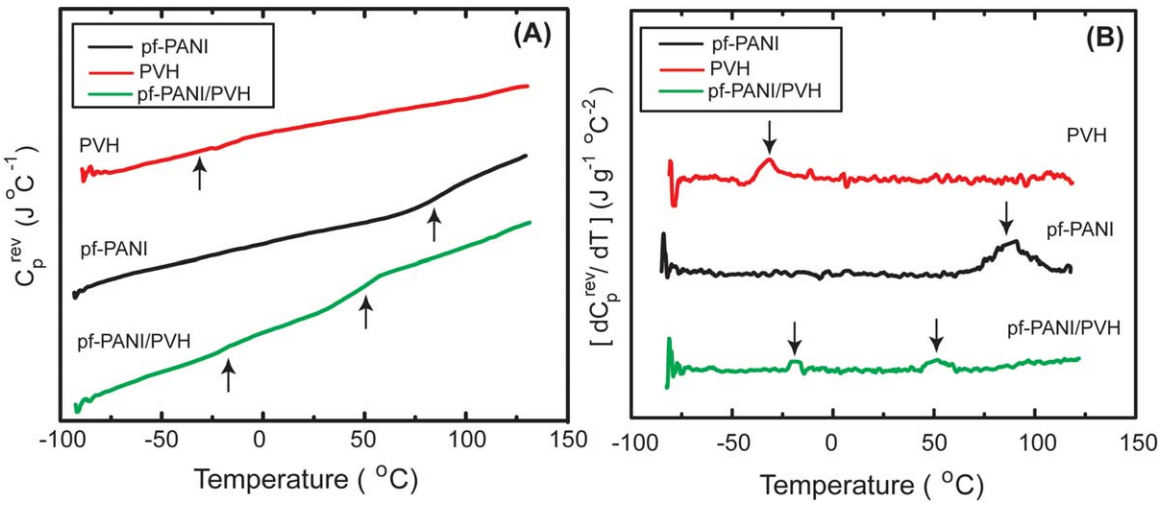


**Figure 5.** Typical MDSC plots for pf-PANI, PVH, and pf-PANI/PVH (A) $C_p^{rev}$ versus temperature and (B) $[dC_p^{rev}/dT]$ versus temperature. The curves have been displaced vertically for clarity. [Color figure can be viewed in the online issue, which is available at wileyonlinelibrary.com.]

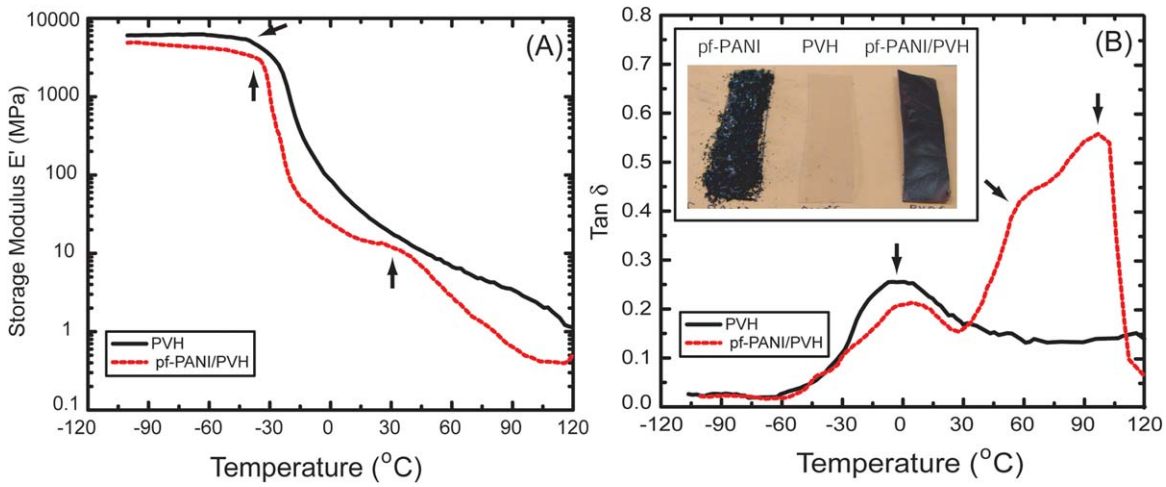


**Figure 6.** The DMTA plots for PVH and pf-PANI/PVH in the temperature range −100°C to 120°C. (A) storage modulus ($E'$) versus temperature and (B) tan $\delta$ versus temperature. The inset in Fig. 10B is the photographs of pf-PANI, PVH, and pf-PANI/PVH. [Color figure can be viewed in the online issue, which is available at wileyonlinelibrary.com.]

using an automatic smooth program, which uses the Savitzky-Golay algorithm (see Figure 7). The main characteristic scattering patterns appear at $2\theta < 45°$ and clearly reveals the effect of pf-PANI on the crystalline phase of PVH. The scattering profile of PVH reveals two sharp diffraction peaks at $2\theta = 18.5°$and 20.1° and a broad diffraction peak at 38.6° as reported for PVH.[46] The scattering peaks seen at $2\theta = 18.5°$ and 20.1° are due to α-crystalline phase of PVDF.[1,47] The pf-PANI reveals a sharp scattering peak at $2\theta = 7.3°$ and a broad scattering peak at ca. $2\theta = 23.6°$. It is to be noted that PANI-EB has been reported to exhibit diffraction peak at $2\theta = 20°$ and 25° while

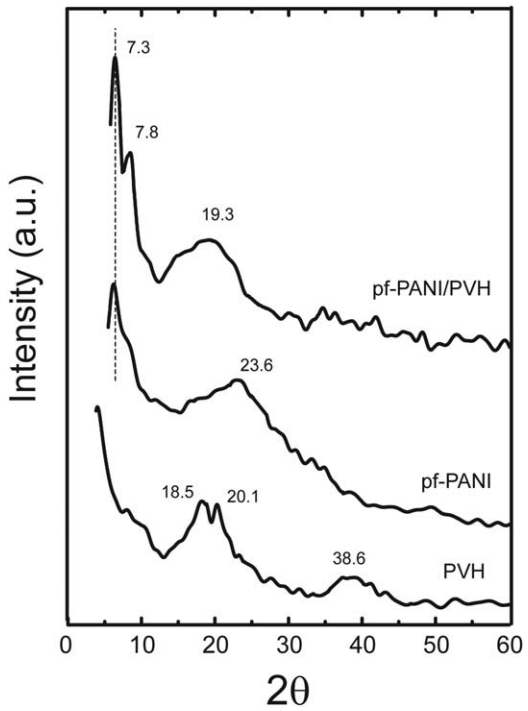


**Figure 7.** XRD scattering profiles of pf-PANI, PVH, and pf-PANI/PVH. For clarity, the scattering profiles have been displaced vertically.

the diffraction peak at ca. $2\theta = 7.3°$ is the characteristic peak of pyrene moiety.[48,49] In our case, it is possible that upon pyrene functionalization the peaks at $2\theta = 20°$ and 25° are not well resolved and seems to exhibit a broad single scattering peak at ca. $2\theta = 23.6°$.

Interestingly, the diffraction pattern of the blend reveals two peaks at low scattering angles one at 7.3° and the other at 7.8°. This new peak at 7.8° indicates the predominance of β-phase of PVDF.[6] We wish to point out here that as reported by some authors,[1,16] we did not observe any separate diffraction peak in the blend near $2\theta = 20°$ that was also associated with the β-phase of PVDF. This could be due to the overlapping diffraction peak of pf-PANI that appears around the same $2\theta$ region thus resulting to a broad scattering hump centered at ca. 19.3° (see Figure 7). Also, in the blend, the diffraction peak at 38.6° seen in PVH almost disappears suggesting that the crystallinity of the PVDF is considerably hindered upon pf-PANI addition. In an earlier XRD study on the blend of PMMA and PVH, the presence of hydrogen bonds between their chains has resulted to decrease in crystallinity which is in consonance with the present results.[47]

In brief, the XRD results reveal that the α-crystalline form of PVH changes to β-form upon blending it with pf-PANI in agreement with FTIR results.[1] It is good to compare here the previous work of PANI blended with PVDF which also resulted to conversion of PVDF crystalline phase from α-form to β-form in agreement with our results.[37] Since the β-crystalline form of PVDF is more polar than α-form,[1,27,37,38] it is easy to realize that it can have good interaction with the polar groups of pf-PANI (see Scheme I). It is to be noted that the FTIR features and XRD peaks assigned for β-phase are quite broad and thus some contributions of α-phase in them could not be ruled out.

### Scanning Electron Microscopy (SEM) Results

The SEM images of the surface morphology of PVH, pf-PANI and the pf-PANI/PVH are displayed in Figure 8(A–C) respectively. The pf-PANI crystals are of irregular shape and are in the

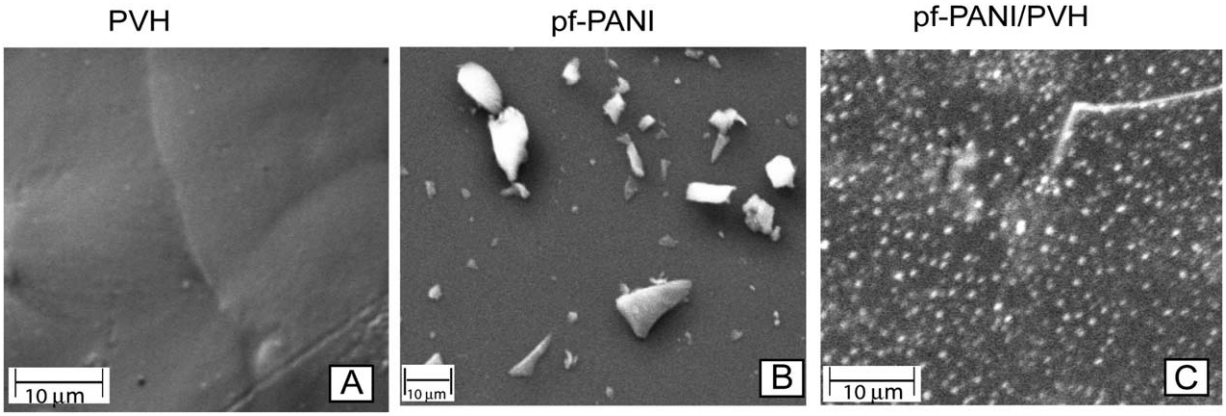


**Figure 8.** The SEM micrographs of (A) pf-PANI, (B) PVH, and (C) pf-PANI/PVH.

size range 2–10 $\mu$m [Figure 8(B)]. However, in the blend, the particle size turns out to be ca. 620 nm and is found uniformly distributed throughout the matrix [Figure 8(C)]. The copolymer acts as an insulation layer between the adjacent conductive pf-PANI particles. More precisely, the blend morphology reveals that the pf-PANI particles are uniformly apart from each other and the space surrounding them is occupied by the dielectric medium. When such a patterned blend is used as a dielectric material, it can impair the occurrence of leakage current, store charges as dielectric and thus can contribute to increase in dielectric permittivity.[17]

### UV–Vis Results

The normalized electronic absorption spectra for pf-PANI, PVH and their blend collected in NMP solution are displayed in Figure 9. The pf-PANI displays a main absorption band at ca. 279 nm while PVH shows no absorption in the wavelength region studied. The electronic absorption of the blend reveals a slight upshift in the wavelength with the main absorption peak appearing at ca. 282 nm. This small up shift in the absorption pattern also supports our findings that the interaction between pf-PANI and PVH exists even in the solution phase.

To understand further details, the UV–Vis spectrum of PANI-EB is also studied. For PANI-EB, the spectrum shows two absorption maxima one at around 330 nm and the other at ca. 630 nm (see inset of Figure 9). The two absorption maxima are attributed to $\pi$–$\pi^*$ transition of the benzenoid and quinonoid form of benzene rings as discussed above.[5,7,21] Please note that the absorption peaks depends on the type of solvent.[5] On the contrary, the absorption spectrum of neither pf-PANI nor the blend showed any absorption at ca. 630 nm. This confirms that the imine part of pf-PANI remains protonated[21,48] by the entrapped HCl during synthesis and is in agreement with the FTIR results.

### Photoluminescence Results

The normalized emission spectrum of the virgin polymers collected in NMP solution is displayed in Figure 10. The PVH exhibits no fluorescence in the wavelength range studied. The pf-PANI exhibits an emission maximum at ca. 421 nm that lies in the purple–blue color region of the visible spectrum with a weak shoulder peak at ca. 480 nm to its right side. The obtained fluorescent intensity pattern is comparable with that reported for pyrene based urethane methacrylate comb polymer and pyrene functionalized Ruthenium nanoparticles.[50,51] The emission bands at lower wavelength (375–395 nm) was reported to be due to electronic transitions of monomeric pyrene moieties and the other at higher wavelength (470–490 nm) was attributed to excimer emission.[50,51] Following this, the main emission peak at 421 nm in pf-PANI could be attributed to electronic transitions of the monomeric pyrene moieties and the shoulder peak at 480 nm to be due to excimer emission. The excimer is a complex which is formed when excited pyrene encounters a ground-state pyrene by processes such as diffusion.[50] If there is a good interaction between the neighbouring pyrene moieties, then this band appears prominent.[50,51] In the present case, the weak shoulder peak at 480 nm implies that there is no significant interaction between the pyrene moieties in pf-PANI. Alternatively, the PL spectrum of pf-PANI in m-cresol exhibits a characteristic emission peak at ca. 479 nm [see Figure 1(B)] implying that there is significant self-

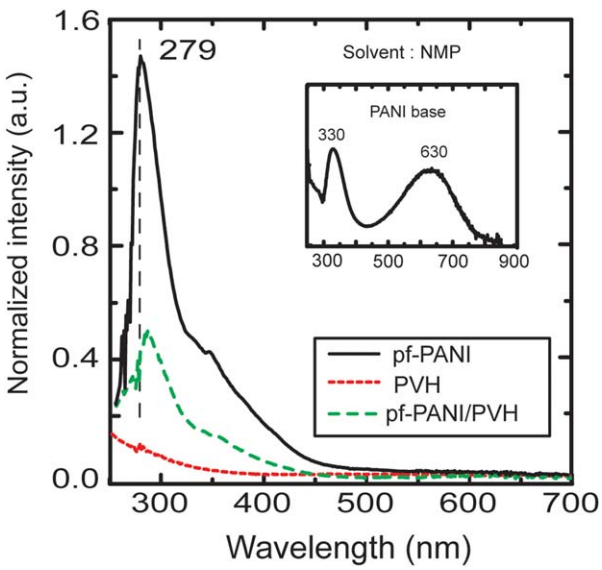


**Figure 9.** Normalized UV–Vis spectrum of pf-PANI, PVH, and pf-PANI/PVH collected in NMP solution (0.01 mg/mL). For comparison, the absorption spectrum of PANI-EB is shown in the inset. [Color figure can be viewed in the online issue, which is available at wileyonlinelibrary.com.]

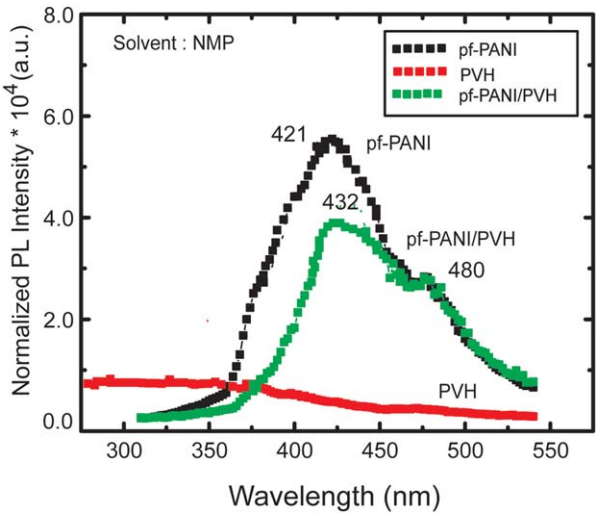


**Figure 10.** Normalized PL spectra of pf-PANI, PVH, and pf-PANI/PVH obtained in NMP solution (0.005 mg/mL). [Color figure can be viewed in the online issue, which is available at wileyonlinelibrary.com.]

aggregation of pyrene moieties and thus shows prominent excimer emission. Thus, in a broader sense, this emission peak at 480 nm reveals information about the nature of the polymer association. Since there is no significant change in the shoulder peak between pf-PANI and its blend (in NMP solvent) implies that blending has not resulted to closure association of hanging pyrene units, which is again an indication of good intermolecular interaction between pf-PANI and PVH.

The peak of emission spectrum for the blend appeared red shifted by 11 nm, which also supports the interaction between the two polymers in the solution phase. It is interesting to note that even a small red shift in the absorption spectrum has resulted to large red shift in the emission spectrum. It has been reported that the pyrene fluoropore suffers from short emission wavelength, which makes it difficult to use in fluorescence imaging applications.[52] Thus, the upshift of emissive wavelength obtained in the present study gains significance.

It is surprising to have such a high intensity PL spectrum in the blend that contains only 50% of the photoactive polymer. From the SEM study, we know that these pf-PANI particles are uniformly distributed and confined to a small region of 620 nm. It is known that pyrene in the aggregated state suffers from reduced-emission due to self-quenching effect.[20] Very recently, significant enhancement in fluorescent intensity of pyrene molecules has been reported and the reason for enhancement is attributed to reduced self-quenching effect upon confining them to nanosizes.[49] Thus, one could speculate that such a nanosize confinement of pf-PANI exists even in the solution phase which could be the reason for high PL intensity in the blend.

From the SEM study, we understand the blend morphology to be uniformly distributed pf-PANI molecules separated by PVH matrix which acts as an insulating medium (dielectric material). In such a pattern, there are very less chances for the particulates to connect with each other to form a conductive network [see Figure 8(C)]. In the absence of percolative paths, the conduction mechanism in this blend could be due to inter-particle tunneling effect as reported in PANI/PVDF nanohybrid films.[17] Differing from the common way of preparation of high dielectric material by the physical dispersion of a ceramic phase in virgin PVH, the polyblends of this type have the advantage of keeping the flexibility inherent in the material. Also, the blend obtained in the form of film is flexible and has stiffness very close to PVH [Figure 6(A,B)]. These results open up relationship between the thermal, microstructure and optical properties of pf-PANI/PVH blends that could help to develop materials with high dielectric constant. A more detailed electrical and dielectric study on this blend is currently under way.

It is known that PVH is a preferred polymer electrolyte compared with PVDF due to its high amorphous nature thus resulting in high ionic conductivity.[35] The developed pf-PANI/PVH blend is more amorphous than PVH and has better damping property especially in the temperature range 40–100°C. The polymer electrolyte film must be thermally stable since heat is generated when used in the battery. Since this blend film has shown thermal stability atleast up to 200°C both in inert and oxidative atmosphere [see Figure 3(A–D)], it is expected that the blend could also find application as a polymer electrolyte.

## CONCLUSIONS

Partially compatible polymers blend using pyrene functionalized PANI has been reported for the first time. The pf-PANI was blended with the copolymer of VDF and hexa fluoropropylene. The $T_g$ of pf-PANI has been identified for the first time to be ca. 85°C by repeated heating–cooling cycles and also confirmed by MDSC measurements. Blending pf-PANI with PVH transforms the PVH from more crystalline $\alpha$ phase to less crystalline $\beta$ phase. The possible intermolecular interaction between the $\rangle$C═O group of pf-PANI and $CH_2$ group of PVH has resulted to a partially miscible pf-PANI/PVH blend. The SEM results reveal that the pf-PANI particles confines to ca. 620 nm size surrounded by high dielectric PVH matrix. The blend is thermally stable atleast up to 200°C, possesses optimum mechanical stability which is much better than the pf-PANI alone. This pf-PANI/PVH blend also being flexible and more amorphous compared with PVH, could find application as a polymer electrolyte.

## ACKNOWLEDGMENTS

The authors thank Dr. A.K. Saxena, Director, DMSRDE, Kanpur for the encouragement and support during this work. The authors are also thankful to Dr. A.S. Singh and Dr. (Mrs.) Swati Chopra for discussions regarding the chemical structure of pf-PANI. One of the authors (VPS), thank DRDO for the financial assistance in the form of a Research Associateship.

## REFERENCES

1. Tiwari, V. K.; Kulriya, P. K.; Avasthi, D. K.; Maiti P. *J. Phys. Chem. B.* **2009**, *113*, 11632.
2. Dias, F. B.; Plomp, L.; Veldhuis, J. B. J. *J. Power Sources* **2000**, *88*, 169.
3. Shi, L.; Wang, R.; Cao, Y.; Feng, C.; Liang, D. T.; Tay, J. H. *J. Membr. Sci.* **2007**, *305*, 215.

4. Saikia, D.; Wu, H.-Y.; Pan, Y.-C.; Lin, C.-P.; Huang, K.-P.; Chen, K.-N.; Fey, G. T. K.; Kao, H.-M. *J. Power Sources* **2011**, *196*, 2826.
5. Malmonge, L. F.; Lopes, G. A.; Langiano, S. C.; Malmonge, J. A.; Cordeiro, J. M. M.; Mattoso, L. H. C. *Eur. Polym. J.* **2006**, *42*, 3108.
6. Malmonge, L. F.; Mattoso, L. H. C. *Polymer* **1995**, *36*, 245.
7. Hwang, G.-W.; Wu, K.-Y.; Hua, M.-Y.; Lee, H.-T.; Chen, S.-A. *Synth. Met.* **1998**, *92*, 39.
8. Rao, P. S.; Subrahmanya, S.; Sathyanarayana, D. N. *Synth. Met.* **2003**, *139*, 397.
9. Ray, S.; Easteal, A. J.; Cooney, R. P.; Edmonds, N. R. *Mater. Chem. Phys.* **2009**, *113*, 829.
10. Segal, E.; Haba, Y.; Narkis, M.; Siegmann, A. *J. Appl. Polym. Sci.* **2001**, *79*, 760.
11. Yang, S.; Ruckenstein, E. *Synth. Met.* **1993**, *59*, 1.
12. Ruckenstein, E.; Yang, S. *Synth. Met.* **2003**, *53*, 283.
13. Rao, P. S.; Subrahmanya, S.; Sathyanaranaya D. N. *Synth. Met.* **2004**, *143* 323.
14. Nand, A. V.; Ray, S.; Travas-Sejdic, J.; Kilmartin, P. A. *Mater. Chem. Phys.* **2012**, *134*, 443.
15. Subramaniyam, C. K.; Kaiser, A. B.; Gilberd, P. W.; Wessling, B. *J. Polym. Sci. Polym. Phys. Ed.* **1993**, *31*, 1425.
16. Malmonge, L.; Mattoso, L. H. C. *Polymer* **2000**, *41*, 8387.
17. Yuan, J. K.; Dang, Z.-M.; Yao, S.-H.; Zha, J.-W.; Zhou, T.; Li, S.-T.; Bai, J. *J. Mater. Chem.* **2010**, *20*, 2441.
18. Lin, S.-C.; Coates, M.; Pearce, E. M.; Huang, P.-T. *Eur. Pat. EP 0 947 556 B1*, Nov 10, **2004**.
19. Amarnath, C. A.; Kim, H. K.; Yi, D. K.; Lee, S.; Do, Y. R.; Paik, U. *Bull. Korean Chem. Soc.* **2011**, *32*, 1495.
20. Figueira-Duarta, T. M.; Müllen, K. *Chem. Rev.* **2011**, *111*, 7260.
21. Wang, P.; Tan, K. L.; Kang, E. T.; Neoh, K. G. *Appl. Surface Sci.* **2002**, *193*, 36.
22. MacDiarmid, A. G.; Chaing, J. C.; Halpern, M.; Huang, W. S.; Mu, S. L.; Somasiri, N. L.; Wu, W.; Yaniger, S. I. *Mol. Cryst. Liq. Cryst.* **1985**, *121*, 173.
23. Vaiyapuri, R.; Greenland, B. W.; Rowan, S. J.; Colquhoun, H. M.; Elliott, J. M.; Hayes, W. *Macromolecules* **2012**, *45*, 5567.
24. Quillard, S.; Louarn, G.; Lefrant, S.; Macdiarmid, A. G. *Phys. Rev. B* **1994**, *50* 12496.
25. Yu, Y.; Che, B.; Si, Z.; Li, L.; Chen, W; Xue, G. *Synth. Met.* **2005**, *150*, 271.
26. Byler, D. M.; Susi, H. *Biopolymers* **1986**, *25*, 469.
27. Gao, Q.; Scheinbeim, J. I. *Macromolecules* **2000**, *33*, 7564.
28. Ramani, R.; Hanski, S.; Laiho, A.; Tuma, R.; Kilpeläinen, S.; Tuomisto, F.; Ruokolainen, J.; Ikkala, O. *Biomacromolecules* **2008**, *9*, 1390.
29. Yongquan, D.; Ming, W.; Lin, C.; Mingjun, L. *Desalination* **2012**, *295*, 53.
30. Ren, Z.; Liu, Y.; Sun, K.; Zhou, X.; Zhang, N. *Electrochem. Acta* **2009**, *54*, 1888.
31. Liu, Y.; Lee, J. Y.; Hong, L. *Solid State Ionics* **2002**, *150*, 317.
32. Jeevananda, T.; Siddaramaiah, Seetharamu, S.; Saravanan, S.; D'Souza, L. *Synth. Met.* **2004**, *140*, 247.
33. Kulkarni, V. G.; Campbell, L. D; Mathew, W. R. *Synth. Met.* **1989**, *30*, 321.
34. Lo, M. Y.; Zhen, C.; Lauters. M.; Jabbour, G. E.; Sellinger, A. *J. Am. Chem. Soc.* **2007**, *129*, 5808.
35. Saikia, D; Kumar, A. *Electrochem. Acta* **2004**, *49*, 2581.
36. Ye, H; Xu, J. J. *J. Power Sources* **2007**, *165*, 500.
37. Bliznyuk, V. N.; Baig, A.; Singamaneni, S.; Pud, A. A.; Fatyeyeva, K. Y.; Shapoval, G. S. *Polymer* **2005**, *46*, 11728.
38. Shubha, N.; Prashanth, R.; Hoon, H. H.; Srinivasan, M. *Mater. Res. Bull.* **2013**, *48*, 526.
39. Malmonge, L. F.; Langiano, S. C.; Cordeiro, J. M. M.; Mattoso, L. H. C.; Malmonge J. A. *Mater. Res.* **2010**, *13*, 465.
40. Wang, Y.-J.; Kim, D. *J Membr. Sci.* **2008**, *312*, 76.
41. Zhao, J.; Ediger, M. D.; Sun, Y.; Yu, L. *Macromolecules* **2009**, *42*, 6777.
42. Sakaguchi, T.; Taniguchi, N.; Urakawa, O.; Adachi, K.; *Macromolecules* **2005**, *38*, 422.
43. Wästlund, C.; Berndtsson, H.; Maurer, F. H. *J. Macromolecules* **1998**, *31*, 3322.
44. Ramani, R.; Alam, S. *J. Appl. Polym. Sci.* **2012**, *125*, 3200.
45. Chen, J.-H.; Zhong, J.-C.; Cai, Y.-H.; Su, W. B.; Yang, Y.-B. *Polymer* **2007**, *48*, 2946.
46. Kumar, G. G.; Kim, P.; Kim, A. R.; Nahm, K. S.; Elizabeth, R. N. *Mater. Chem. Phys.* **2009**, *115*, 40.
47. Ding, Y.; Zhang, P.; Long, Z.; Jiang, Y.; Xu, F.; Di, W. *J. Membr. Sci.* **2009**, *329*, 56.
48. Anilkumar, P.; Jayakannan, M. *Langmuir* **2008**, *24*, 9754.
49. Lo, K.-H.; Li, M.-C.; Ho, R.-M.; Zhao, Y.-C.; Massuyeau, F.; Chuang, W.-T.; Duvail, J.-L.; Lefrant, S.; Hsu, C.-S. *Langmuir* **2013**, *29*, 1627.
50. Deepak, V. D.; Asha, S. K. *J. Phys. Chem. B.* **2009**, *113*, 11887.
51. Chen, W.; Zuckerman, N. B.; Lewis, J. W.; Konopelski, J. P.; Chen, S. *J. Phys. Chem. C.* **2009**, *113*, 16988.
52. Bag, S. S.; Kundu, R. J. *Org. Chem.* **2011**, *76*, 3348.